

HEAM : Hashed Embedding Acceleration Using Processing-In-Memory

Youngsuk Kim, Hyuk-Jae Lee, Chae Eun Rhee

Abstract—In today’s data centers, personalized recommendation systems face challenges of large memory capacity requirements and high memory bandwidth demand, especially for embedding operations. Previous approaches have relied on DIMM-based near-memory processing techniques or introduced 3D-stacked DRAM to address memory-bound issues. However, these solutions fall short when dealing with the expanding size of personalized recommendation systems. Recommendation models have grown to sizes exceeding tens of terabytes, making them challenging to run efficiently on traditional single-node inference servers. Although various algorithmic methods have been proposed to reduce embedding table capacity, they often result in increased memory access or inefficient utilization of memory resources.

This paper introduces HEAM, a heterogeneous memory architecture that integrates 3D-stacked DRAM with DIMM to accelerate recommendation systems in which compositional embedding is utilized—a technique to reduce the size of embedding tables. The architecture is organized into a three-tier memory hierarchy consisting of conventional DIMM, 3D-stacked DRAM with a base die-level Processing-In-Memory (PIM), and lookup tables inside bank group-level PIM. This setup is specifically designed to accommodate the unique aspects of compositional embedding, such as temporal locality and embedding table capacity. This design effectively reduces bank access, improves access efficiency, and enhances overall throughput, resulting in $6.2\times$ speedup and 58.9% energy savings compared to the baseline.

Index Terms—Processing in memory, recommendation system, compositional embedding, heterogeneous memory, 3D-stacked DRAM.

I. INTRODUCTION

PERSONALIZED recommendation system serves as an essential technology of various companies such as Meta [1], YouTube [2] and Netflix [3]. Recently, deep learning-based recommendation systems have emerged as a pivotal technology for improving the accuracy of predicting user-preferred content, thereby contributing to enhanced profitability for these companies. These advanced recommendation systems currently contribute substantially to the computational workload of the data center. Recent reports indicate that approximately 80% of data center resources are dedicated to the inference process of recommendation systems [4]. Recommendation models use dense features for user information and sparse features for item specifics through embedding operations. Following feature interactions, multi-layer perceptron

(MLP) layers generate click-through-rate (CTR) predictions, estimating the likelihood of user clicks on recommended items.

In large-scale data centers that extensively utilize embeddings, the embedding operation often becomes the primary factor influencing overall system performance. This stems mainly from the operation’s tendency to exhibit sparse and irregular memory access patterns. As a result, these memory-bound operations place significant constraints on traditional data center infrastructures [5], and this challenge continues to grow with the scale, as depicted in Figure 1. To tackle this challenge, recent efforts have concentrated on designing memory systems tailored to embedding operation [6], [7], [8], [9], [10], [11]. Approaches like TensorDIMM [6] and RecNMP [7] have explored the effectiveness of incorporating near-memory-processing (NMP) to alleviate the memory-bound nature by accelerating embedding operations directly within off-chip memory. These architectural solutions expedite the gather-and-reduce (GNR) process of embedding operations by deploying processing units in each rank of Dual Inline Memory Module (DIMM). This approach effectively harnesses the internal memory bandwidth, further amplified by the number of ranks in the memory channel. TRiM [8] and SPACE [9] followed a similar NMP structure while introducing other modifications to memory architecture. TRiM employed bank group-level processing-in-memory (PIM) within the DRAM device, while SPACE utilized High Bandwidth Memory (HBM) [12] as a Dynamic Random Access Memory (DRAM) cache.

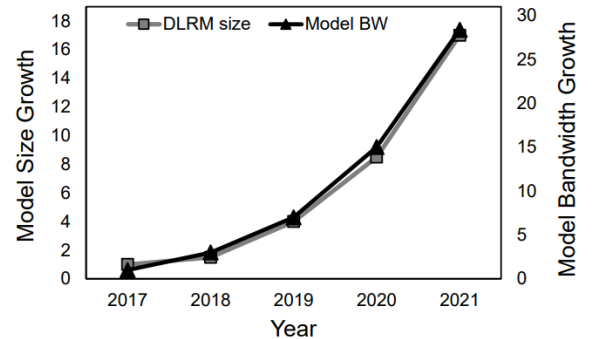


Fig. 1. Model size and bandwidth growth of DLRM. (Reproduction from RecShard [13])

On the other hand, personalized recommendation models are currently expanding in its size. According to RecShard [13], the memory capacity requirement of the Deep Learning Recommendation Model (DLRM) has been enlarged 16 times from 2017 to 2021, as shown in Figure 1. The model’s growth is attributed to the fact that incorporating more items attributes

Youngsuk Kim and Hyuk-Jae Lee are with the Inter-University Semiconductor Research Center (ISRC), Department of Electrical Engineering and Computer Science, Seoul National University, Seoul 08826, South Korea (e-mail: youngsuk95@capp.snu.ac.kr; hjlee@capp.snu.ac.kr).

Chae Eun Rhee is with the Department of Electronic Engineering, Hanyang University, Seoul 04736, South Korea (e-mail: crhee@hanyang.ac.kr).

to better model quality [13], [14]. However, the model operating on the inference server [5], [15], [16], [17] is significantly smaller in scale compared to the training model [13], [14]. Therefore, a significant gap exists between the training model size and the inference model size. Serving the inference with a multi-node server or introducing Solid-State-Drivers (SSDs) could be a possible solution. However, it comes at the cost of synchronization and vulnerability to failures for the multi-node server case, and the SSDs have a negative impact on execution time [15], [18]. Therefore, exploring an alternative approach is essential to optimize model inference without encountering these drawbacks. Prior works took algorithmic approaches to reduce the embedding table size [19], [20], [21], [22]. While these techniques have successfully reduced the size of the embedding table, their work has been done at the cost of imposition of a much heavier burden on the memory bandwidth or inefficient memory capacity management. A representative method is compositional embedding [19], which employs a simple double-hashing technique to transform the original embedding table into a smaller quotient (Q) table and remainder (R) table. Nevertheless, this method necessitates double memory access, amplifying the memory-bound characteristics.

We propose HEAM, a specialized memory architecture integrated with PIM technology, designed to accelerate the inference process of compositional embedding. HEAM introduces a three-tiered memory hierarchy consisting of DIMM, HBM, and a lookup table (LUT). HBM is incorporated with base-die PIM (bd-PIM), and bank-group PIM (bg-PIM), and LUT that serves as an additional storage space within bg-PIM. This design is based on the following observations. Similar to the original embedding, the Q table exhibits high temporal locality characteristics within a small portion of the entire embedding vector. Therefore, HEAM leverages HBM and DIMM to exploit this temporal locality, storing high temporal locality vectors to the HBM and others to the DIMM. Notably, the R table, in particular, has a very small size and demonstrates a remarkably high temporal locality. Hence, we utilize an LUT within bg-PIM to store the entire R table. By addressing the memory bandwidth challenges associated with compositional embedding, HEAM effectively reduces the size of the embedding tables while simultaneously satisfying the requirements for memory bandwidth. This capability enables the execution of large models on a single-node server at a high processing speed. The primary contributions of our work can be summarized as follows:

- To the best of our knowledge, HEAM is the first work to address both the large model size problem and the memory-bound issue of the DLRM. HEAM successfully tackles both issues by designing specialized hardware for compositional embedding.
- We propose an allocation strategy for each hash table in compositional embedding. By distinguishing storage space for each table based on the analysis of their unique characteristics, HEAM achieves additional gains in bandwidth.
- We design a two-level PIM within HBM, specifically tai-

lored for compositional embedding. This enables HEAM to expand into a three-tiered memory system, incorporating DIMM, HBM, and the LUT within PIM, thus effectively enhancing memory parallelism. Using LUT facilitates the additional speedup of Processing-In-Memory (PIM) architectures.

II. BACKGROUND

A. Personalized Recommendation System

Recommendation System Overview. Among the various personalized recommendation models employed by diverse companies, DLRM stands out as one of the prominent recommendation system models. In the DLRM framework, inputs are categorized into two groups: dense features and sparse features. Dense features correspond to user information expressed as floating-point values, while sparse features facilitate access to items by transforming them into embedding vectors that encapsulate item-specific features. Figure 2 provides an illustration of the DLRM architecture. The bottom-mlp takes dense features as inputs, while the embedding lookup process handles sparse features. The embedding lookup operation gathers individual embedding vectors from multiple embedding tables, generating a single reduced vector. This reduced embedding vector is subsequently concatenated with the outcome of the bottom-mlp through a feature interaction layer. The resulting combined representation is then fed into the top-mlp. Once the top-mlp completes its calculations, the final outcome, CTR, is generated.

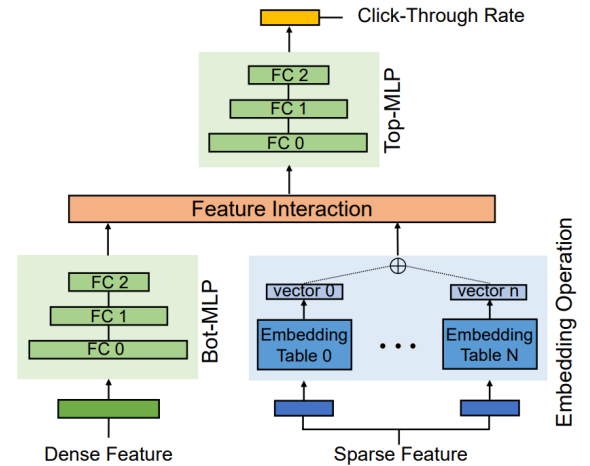


Fig. 2. DLRM architecture

Challenges in Recommendation System Inference. The performance of the recommendation system is constrained by the memory-bound nature of the embedding operation. The irregular access patterns of embedding vectors, combined with the extensive size of the embedding table that surpasses the cache storage capacity on the host side, necessitate the frequent look-up of embedding vectors from the off-chip memory system. This frequent access to main memory leads to higher latency for the embedding operation than that of the bottom-mlp [9], classifying the model as memory-bound.

Recently, recommendation models have been trending towards incorporating increasingly large-sized embedding tables, with their scale growing year by year [13]. Nowadays, industry-scale DLRM implementations require substantial memory resources, often reaching sizes of up to tens of terabytes, a significant portion of which is dedicated to housing embedding tables [15], [5]. Given that the quality of the model is closely linked to the size of these embedding tables, there is a strong incentive to utilize as large embedding tables as possible in production. However, the practical utilization of such large models is constrained by physical limitations, as the memory size of a single-node server is restricted by the available slots within the server.

B. Algorithms for Reducing Embedding Data Size

Algorithms Overview. Table I presents a comparison between aspects of algorithmic approaches for reducing embedding table size, including compression rates (Compression), accuracy relative to the original model (AUC), and operational characteristics such as bandwidth bound (BW bound) and memory friendliness (Mem. friendly). These methods could be categorized into three groups: Parameter Sharing (PS), Mixed Dimension (MD) and Generative Embeddings (GEN). The PS group utilizes hashing methods that map consecutive embedding vectors to the same vector. Conversely, MD group focuses on eliminating redundancy within the embedding dimensions, where embedding vectors that have minimal impact on the output are resized to a smaller dimension. The GEN group generates embedding from input indices using compute-intensive operations such as MLP, instead of storing embedding vectors as data. The PS group offers advantages regarding memory efficiency as its methods produce vectors with uniform dimensions as the algorithm’s output, promoting efficient utilization of memory capacity and accommodating memory system bursts effectively. However, the drawback is that the accuracy lags behind the baseline due to the semantic overlap among non-relevant embedding vectors. Furthermore, the degree of compression achieved is relatively modest. The MD and GEN groups attain a high compression rate and better model accuracy than the baseline. In the MD group, however, efficient use of memory resources is relatively hard since the output vectors vary in their dimension. Finally, the GEN group transforms the target model into the compute-bound application, which is far from the memory perspective, in contrast to other memory-bound groups.

TABLE I
COMPARISON OF EMBEDDING TABLE REDUCTION SCHEMES.

Group	Method	Compression	AUC	BW bound	Mem. friendly
PS	Hashing [23]	Low	Much Lower	Memory	✓
	QR [19]	Moderate	Lower	Memory	✓
MD	MDE [20]	Moderate	Better	Memory	✗
	OptEmbed [22]	High	Better	Memory	✗
GEN	TT-Rec [21]	High	Better	Compute	✗
	DHE [24]	High	Better	Compute	✗

Compositional Embedding. Compositional embedding employs two types of hash functions, effectively partitioning

each of the original embedding tables into two smaller tables, as depicted in Figure 3 (a). These hash functions consist of quotient and remainder operations, where the original embedding vector index is used as an input. Embedding vectors that yield the same quotient value, that are consecutive embedding vectors, are mapped to corresponding vectors in the table generated by the quotient function (Q table). On the other hand, embedding vectors with identical remainder results, which departed from each other with the distance of hash collision value, are directed to the same vector within the other hash table (R table). To process the embedding operation, it is necessary to reconstruct the original embedding from Q table and R table. This is accomplished by performing straightforward mathematical operations on the vectors extracted from each table. The overall scheme is illustrated in Figure 3 (b). Note that the user may select reconstruction operation among addition, multiplication and concatenation[19]. The total table size is reduced by a factor approximately equal to the inverse of the hash collision. The R table size is usually negligible compared to the Q table, as its size corresponds to the hash collision. In contrast, the Q table size is equivalent to the original table size divided by the hash collision.

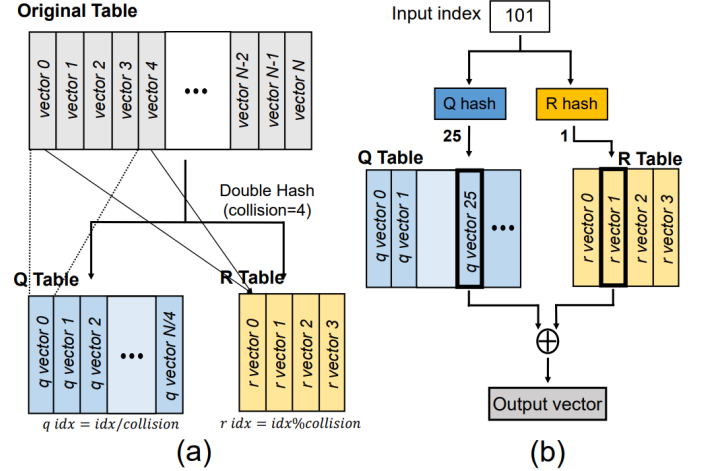


Fig. 3. Compositional embedding overview. (a) Double hashing process (b) Embedding vector reconstruction process

C. NMP/PIM Designs for Recommendation System

Recent studies have introduced NMP units within the DRAM architecture to meet the memory bandwidth requirements of recommendation systems. Specifically, these approaches have incorporated multiple DIMMs with NMP units situated within their DIMM/Rank configurations, effectively exploiting DIMM/Rank-level parallelism [6], [7] to achieve increased throughput. TRiM [8] focused on the tree topological structure of the DRAM’s data path, further enhancing parallelism by integrating PIM units within each bank group. In these previous designs, NMP/PIM operations are not executed in a synchronized style as embedding vectors are accessed randomly. However, as each vector read requires more than one DRAM read access cycle (tRAS), a new NMP/PIM operation could be successfully transferred and

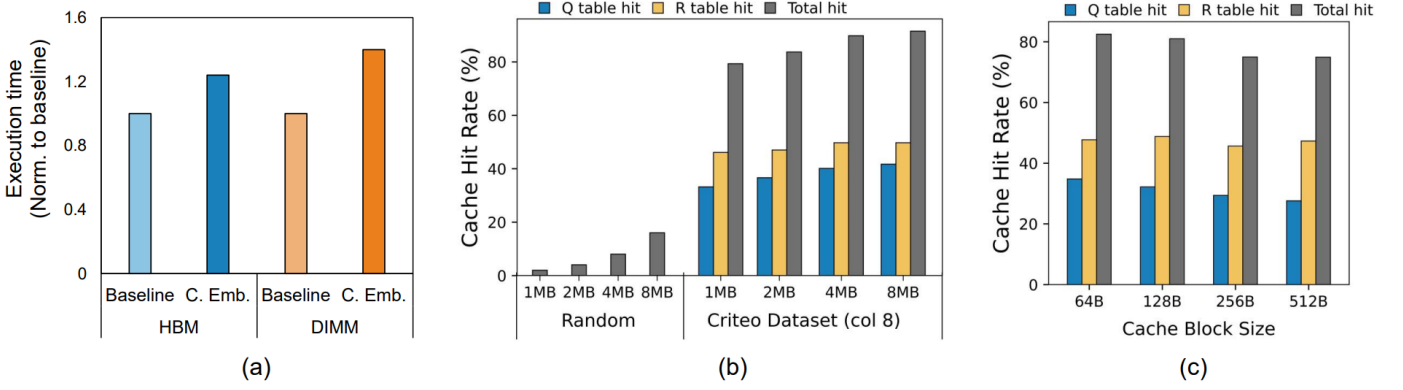


Fig. 4. Compositional Embedding Analysis (a) Execution time comparison between original DLRM and compositional-embedding-applied DLRM (b) Verifying temporal locality by increasing cache size from 1MB to 4MB with vector length of 64B (c) Spatial locality by increasing cache line size from 64B to 512B where cache size is fixed to 1MB with vector length of 64B

initiated before the previous instruction in another NMP/PIM unit completes, resulting in parallel executions. In pursuit of additional speedup, the aforementioned designs have leveraged the long-tail distribution of embedding vectors, where a small subset of embedding vectors is frequently reused. This has been accomplished by incorporating a cache within the buffer chip [7] or implementing load-balancing techniques with the assistance of the memory controller [8].

While it is possible to increase the throughput of the embedding operation by incorporating more DIMMs with NMP designs from previous approaches, this may lead to inefficiencies in power consumption [9]. To address this challenge, SPACE [9] introduced a heterogeneous memory system that combines HBM and DIMMs, with HBM functioning as a DRAM cache. Additionally, SPACE exploited the reduction locality of embedding vectors and the long-tail distribution of embedding vectors to achieve significantly higher throughput. In summary, achieving high performance in recommendation systems relies on core techniques that involve exploiting parallelism within the main memory and capitalizing on the long-tail distribution of embedding vectors.

III. ANALYSIS ON COMPOSITIONAL EMBEDDING

As shown in Section II-B, compositional embedding exhibits several advantages over other previously proposed schemes concerning the memory system. While alternative methods may yield better model prediction quality and higher compression rates, the nature of the output data poses challenges for the memory system when supporting the embedding operation efficiently. Consequently, we have selected compositional embedding as the target algorithm. In this section, we offer an in-depth analysis of the characteristics of compositional embedding.

A. Impact on DLRM Throughput

Compositional embedding further intensifies the memory-bound characteristics of the model by doubling the overall number of accesses to the main memory. This is because generating input vectors for the model necessitates access to two hash tables. Figure 4 (a) presents a comparison of the

execution times for embedding operations on HBM and DIMM between the original model and the model with compositional embedding applied. The results indicate that compositional embedding leads to a 25% longer execution time on HBM and a 40% longer execution time on DIMM. Although the decrease in throughput is less pronounced on HBM due to its significantly higher number of channels compared to DIMM, it is evident that employing the compositional embedding results in increased memory access. This underlines the need for higher bandwidth than what traditional memory systems can provide.

B. Temporal and Spatial Locality

To investigate the locality characteristics in compositional embedding, we simulated cache behavior with embedding traces from criteo-kaggle-dataset [25]. A 4-way set associative cache is used during the experiment. Note that MLP weights are not included during the simulation, thereby producing a high cache hit rate of embeddings.

Temporal Locality. To find out the presence of temporal locality, we followed the method used in RecNMP [7]. We increased cache size from 1MB to 8MB and examined the difference in hit rate of random traces and traces generated from criteo dataset [25], [26] with compositional embedding applied, as depicted in Figure 4 (b). The total hit rate of compositional embedding is the summation of Q table and R table hit rate, which is much higher than that of the random traces. This result implies the temporal locality characteristics of double-hashed embeddings. Although hit rate of Q table is slightly smaller than R table, it is still much higher compared to random traces, indicating strong temporal locality of Q table embeddings, resembling original table locality characteristics that is examined in prior works [7], [9]. This is due to the similar long-tail distribution between the original and the Q table, as illustrated in Figure 5. According to Figure 5 (a), a small subset of total embeddings takes the majority of the access. We refer to this subset as *hot vectors*. When quotient hashing maps consecutive embeddings to the same embedding, hot vectors tend to remain as hot vectors since the access rate of Q table embedding is identical to the access rate summation

of consecutive embeddings that are mapped to that Q table embedding. Therefore, long-tail distribution remains similar as shown in Figure 5 (b).

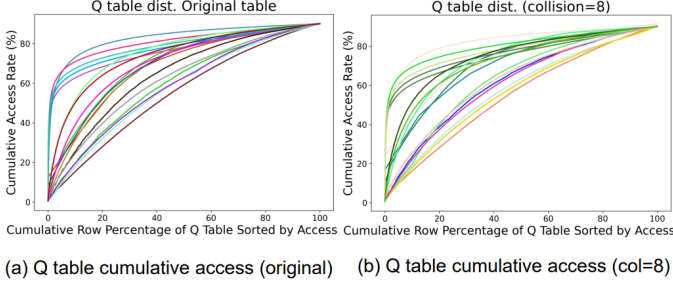


Fig. 5. Cumulative access distribution of tables. (a) Original table (b) Q table with hash collision=8.

As depicted in the Figure 4 (b), R table cache hit rate occupies fixed, high portion of the total hit rate across all the cache size. This indicates each vector inside R table presents high temporal locality. The main reason is that R table size is smaller than that of the Q table, even though both tables are accessed concurrently to construct the input embedding. This concentrates R table access on a small number of embeddings, significantly increasing temporal locality. It is worth noting that R table embeddings display uniform locality distribution as illustrated in Figure 6, which is more intensified when hash collision is low. Since the hot vectors are randomly widespread across the embedding table, the remainder hash function maps hot vectors randomly to the R table embeddings. Coupled with the fact that total locality of the R table is high, uniform access distribution of R table embeddings indicates that all the R vectors are hot vectors.

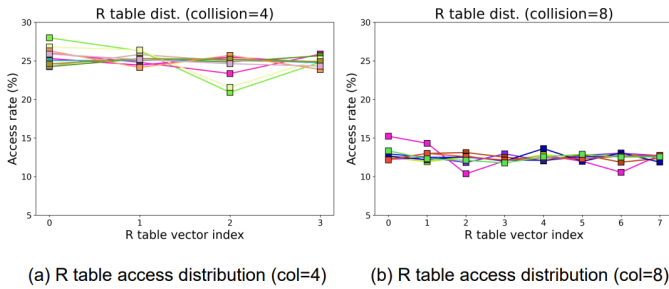


Fig. 6. R table access distribution of 10 embedding tables. (a) Distribution with the collision of 4 (b) Distribution with the hash collision of 8. All embeddings have similar access distribution.

Spatial Locality. The simulation on spatial locality was conducted by measuring the hit rate of 64B length vector on 1MB cache, varying the cache line size from 64B to 512B on 1MB cache, again following the method used in [7]. Results are shown in Figure 4 (c). The observation shows that Q table cache hit rate decreases slightly, indicating little spatial locality. However, the R table cache hit rate implies that a mild spatial locality exists since the overall cache hit rate is stable, even though increasing cache line size diminishes the effect of temporal locality, suggesting the existence of spatial locality. Despite the presence of R table spatial locality, it is challenging to benefit from such characteristics as its

impact is minimal. Furthermore, the embedding dimension exceeds traditional cache line size, as the vector length utilized in the recommendation system typically ranges from 64B to 512B. Fetching multiple R table vectors within a cache line is impossible, although R table vectors might be placed next to each other.

C. Opportunities for PIM Support

The above assessments suggest that enhanced throughput support is necessary for running compositional embedding during the inference stage. Inspired by the previous works that utilize NMP/PIM to extend the bandwidth [6], [7], [8], we conclude that employing PIM is an effective solution for addressing the memory-bound characteristic of compositional embedding. Two attributes of compositional embedding make the usage of PIM more effective. First, as described in Section II-B, the data arrangement is suitable enough to employ the PIM architecture. This is due to the uniformity in vector dimensions, which ensures efficient use of memory capacity and consistency in the total DRAM burst needed for each vector. Second, unique features of the R table vectors, high temporal locality, and its uniform memory access distribution could be efficiently exploited by extending the PIM design to increase the throughput further. Integrated with a heterogeneous system consisting of HBM and DIMM with base die PIM, the utilization of PIM is an effective design for supporting compositional embedding.

IV. HEAM ARCHITECTURE

A. Architecture Overview

We propose HEAM, a specialized memory system designed to enhance the bandwidth of DLRM when compositional embedding is employed. For the reconstruction operation of compositional embedding, addition is utilized in our system. The overall architecture is depicted in Figure 7. As illustrated in Figure 7 (a), the HEAM system incorporates a heterogeneous memory architecture that comprises HBM and DIMM, which addresses the memory-bound nature to some extent by offloading frequently accessed vectors to HBM. Nonetheless, it's important to note that the overall memory access demands double when employing compositional embedding. As a result, depending on conventional HBM remains insufficient to achieve the required throughput.

To tackle this problem, we design a two-level PIM system within the HBM to enhance the throughput by utilizing in-memory parallelism, thereby providing additional bandwidth support for the embedding operation. In Figure 7 (b), the first-level processing unit is located on the base die of the HBM, whereas the second-level processing units are located inside each bank group. These processing units are referred to as bd-PIM and bg-PIM, named based on their respective locations. Within these PIMs, the embedding operation is processed in a two-stage partial addition fashion. Initially, each bg-PIM collects Q embeddings and R embeddings from its dedicated bank group. Local addition is performed inside each

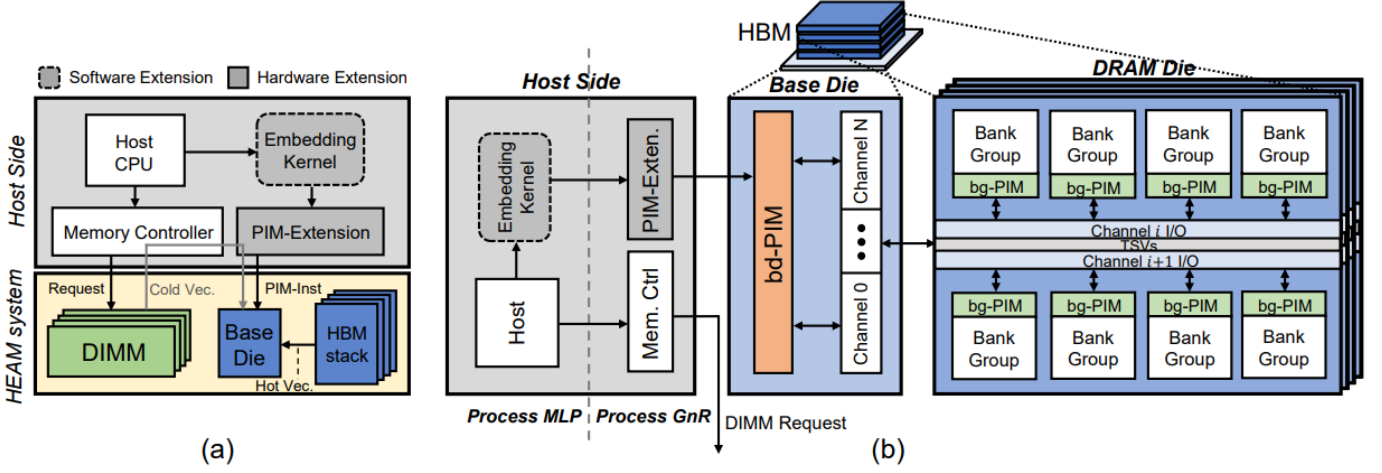


Fig. 7. HEAM architecture. (a) Overview of HEAM architecture, (b) 2-level PIM system in HBM

bg-PIM on the collected embedding vectors, generating partial results. Note that Q embeddings and their corresponding R embeddings don't have to be located in the same bank group, as addition operation is employed, resulting associative law property to be held in the operation. Once all bg-PIMs complete their respective operations, all the reduced vectors are forwarded to the bd-PIM. The same operation is carried out within the bd-PIM for each set of partial results, resulting in the final output delivered to the host processor.

Figure 8 (b) depicts the PIM architecture of bg-PIM. The system inside bg-PIM is equipped with an instruction register, an instruction decoder and a multiply-and-accumulate (MAC) unit. Additionally, LUT is integrated inside each bg-PIM to leverage the temporal locality of the R table described in Section III-B. Therefore, the access to R embedding vectors is always directed to the LUT, decreasing the total bank access. HEAM employs batching of 4 embedding operations to address the load imbalance issue, following the technique utilized in RecNMP [7]. Batching compensates load imbalance issue of the embedding lookup, and the level of compensation increases with large vector size as operation overlap cycles between bank group also increases. To avoid introducing too much area overhead into bank groups, we use up to 4 batch in our system. The bd-PIM receives partial sums delivered from bg-PIM and processes the final GnR operation as illustrated in Figure 8 (a). Note that the architecture of the bd-PIM is similar to that of the previous works.

B. Hash Table Allocation Strategy

To mitigate the double memory access problem associated with compositional embedding, we store the Q and R tables in memory in different ways. This is based on the data access patterns for each table are distinct and exhibit significant variation. Consequently, we ensure more efficient use of memory system resources. As these data access patterns are established after training, we collect this distribution information prior to entering the inference stage. This process incurs minimal overhead in time, as demonstrated in previous studies [7], [9].

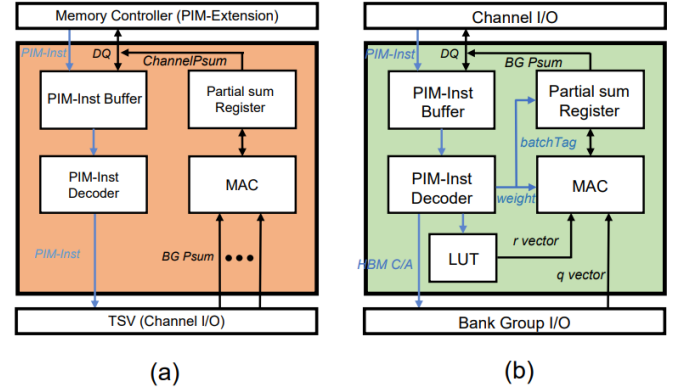


Fig. 8. PIM architectures. (a) bd-PIM, (b) bg-PIM

Mapping Scheme for Q table. As the Q table typically exhibits a long-tail distribution similar to that of the original embedding table, we leverage an approach inspired by SPACE [9] to exploit the Q table's characteristics. Q embeddings with high temporal locality is offloaded to HBM, while the remaining Q embeddings are stored in DIMMs. The proportion of data to be offloaded to HBM is determined based on the bandwidth ratio between HBM and DIMM. This strategy, which involves gathering embedding data with high locality from HBM and fetching the rest from DIMMs, enhances the overall parallelism between the different memory types.

Mapping Scheme for R table. As described in Section III-B, access to the R table is repeatedly conducted for a very limited set of data, consequently, all the data within the R table exhibits extremely high temporal locality. Based on the observation, HEAM stores all the R table embeddings inside the LUT that is located in each bg-PIM. Access to R embeddings are directed to the LUT inside the bg-PIM as depicted in Figure 8 (b). As a result, the number of bank accesses in compositional embedding is reduced by half, making the total number of accesses equivalent to that of the original model. Additionally, given that the R embeddings follow a uniform distribution, load balance between LUT

entries is achieved automatically. The total area overhead of LUT is minimal, as the number of entries required within the LUT is typically small considering the hash collision is usually set as a value less than 60 [19]. As we employ simple addition for input embedding reconstruction operation, we evenly allocate all the R tables across all LUTs in a random fashion without forcing the Q table and R table to be placed within the same bank group.

While bd-PIM could also be considered for LUT placement, bg-PIM offers distinct advantages for extending reconstruction operations for multiplication and concatenation case, as those cases require q vector and its corresponding r vector to be located within the same bank group since associative law doesn't hold in those operations.

C. Advantage of HEAM System in Hash Collision Value

In the HBM-only scenario, when the model size is larger than HBM capacity, additional stacks should be introduced to avoid high hash collision value that might lead to excessive model quality drop of the model. However, this comes at the cost of redundant bandwidth. Employing an HBM-DIMM heterogeneous system is a better approach as it achieves the same hash collision without extra redundant bandwidth. To fully reap the maximum bandwidth of a heterogeneous memory system, each memory request ratio has to be equal to the bandwidth ratio, as displayed in the equation 1.

$$\frac{Request_{HBM}}{Request_{DIMM}} = \frac{BW_{HBM}}{BW_{DIMM}} \quad (1)$$

However, when HBM bandwidth is expanded with PIM, the overall HBM request should be enlarged to meet the above equation, which forces additional data offloading to the HBM. If total data is increased more than HBM capacity, this might demand higher hash collision, leading to decreased model quality. Nevertheless, long tail distribution compensates for such problems as increasing cumulative requests of HBM requires a small amount of additional data. Therefore, there is no need to introduce extra hash collision to meet the bandwidth demand.

D. PIM Instructions and the Execution Flow

PIM Instructions. HEAM leverages the PIM instruction to deliver embedding operation information to each bg-PIM, following RecNMP [7] and TRiM [8]. The total width of a single PIM instruction is 81 bits. The *opcode* (3-bit) specifies the operation type that bd-PIM and bg-PIM should take into action for GnR operation. The *target address* (33-bit) denotes the start address of the PIM-Inst to read from the bank group. *nRD* (4-bit) indicates the vector size. The *weight* (32-bit) delivers weight information for weighted sum. *transfer* (1-bit) determines whether the partial sum is complete and ready to deliver. The *skewed-cycle* (6-bit) instructs bg-PIM the time that PIM instruction should be decoded after being delivered to the bg-PIM. The *batchTag* (2-bit) is the assigned batch of the PIM instruction.

Execution Flow. To run the PIM system, it is essential for the memory controller to deliver PIM instructions to

the memory system properly. Like prior works [7], [8], [9], HEAM offers an embedding operation driver that extends the current memory controller. The driver receives an embedding operation from the host, constructs PIM instructions, and offloads it to the NMP at the HBM. When HBM is used as a DRAM cache inside a heterogeneous memory system, a mapping of data is required to be stored inside the memory controller to direct each of the commands to the proper memory system. To support this, embeddings are mapped with a direct mapping method. With the aid of the direct mapping method, the memory controller could send PIM instructions and DDR4 commands to each memory by leveraging the method used in SPACE [9]. To avoid the cache coherence issues, we allocate memory space dedicated to HEAM as uncachable. Additionally, to cope with the command/address (C/A) bandwidth overhead issue addressed before [8], we follow the method of prior works that utilize data (DQ) pins to deliver a number of instructions to bg-PIMs within a short cycle. Specifically, we utilize 14 C/A pins with 128-bit wide DQ pins to transfer 1 PIM instruction in a single cycle. Due to the abundant HBM DQ pins, HEAM successfully addresses the C/A bandwidth overhead.

V. EXPERIMENTAL SETUP

Simulation Methodology. We modified DRAMsim3 [27], a cycle-accurate memory simulator, to implement and evaluate the performance of the HEAM system and the prior works. HBM2 x128 and DDR4-3200 x8 were utilized as base memory systems for the HEAM system and the baselines. Table II summarizes the memory system configuration utilized in our experiment. Within a single DDR4-3200 x8 device, 2 ranks were employed. To utilize the heterogeneous memory systems, HEAM makes use of a flat addressable method, which has been continuously adopted in prior works on the same system configuration [9], [28], [29], [30]. We compare HEAM performance against previous NMP architectures, TensorDIMM [6], RecNMP [7], TRiM [8] and SPACE [9]. The traces of embedding operation were extracted from running the DLRM model, which is fed into the simulation framework.

TABLE II
MEMORY SYSTEM CONFIGURATIONS

HBM2 x128 device	
Organizations	8 channels per 4-hi stack, 4 bank groups per channel
Timing parameters	tCL=14, tRP=14, tRCD=14, tCCD_S=1, tCCD_L=2, tBL=16
Clock frequency	1000MHz
DDR4-3200 x8 device	
Organizations	1 channel per DIMM, 2 ranks per channel, 4 bank groups per rank
Timing parameters	tCL=22, tRP=22, tRCD=22, tCCD_S=4, tCCD_L=8, tBL=8
Clock frequency	1600MHz

In order to meet fair comparison, we treat all the embeddings within the R table as hot vectors so that temporal locality utilization techniques proposed in prior works could be

maximally exploited. For instance, R table embeddings have the highest priority when participating in *hot entry profiling* when implementing TRiM. In this case, vectors counted from the front of q vectors that are ordered with highest locality takes participation in hot entry profiling after the R table. To fairly measure the performance of SPACE, *reduction locality* technique was employed, storing partial sums of hot vectors in the available space on HBM2. For RecNMP, we linearly scaled the speedup of RankCache, following TRiM.

Area and Power Consumption. To obtain the area overhead and the power consumption of PIM units, bd-PIM and bg-PIM were synthesized using Synopsys Design Compiler with 45nm CMOS technology operating at 300MHz clock frequency. For the case of bg-PIM, the corresponding area was scaled to a 20nm DRAM processing. Area and the power of LUT were estimated using CACTI [31].

Recommendation System Datasets. Obtaining a sufficiently large dataset is crucial for our experiment as HBM2 capacity needs to be fully occupied even after compositional embedding is applied regarding the assumption of the HEAM system. However, since datasets meeting such constraints is not publicly available, we generate synthetic traces from criteo datasets [25], [26] by adjusting their vector sizes between 128B and 512B. Total embedding lookup per operation was set to 78. Note that criteo-terabyte dataset [26] capacity is near 10 GB when the vector length is 64B.

VI. EVALUATION RESULT

We evaluate the impact of HEAM’s design choices as the first step to analyze the effectiveness of each choice. We then compare the performance of HEAM with state-of-the-art NMP designs, which target the embedding operation. Additionally, area overhead and power consumption introduced to the overall system for HEAM architecture support are analyzed. Furthermore, we assess the limitations of compositional embedding to explore the boundary in terms of compositional embedding could be applied to our system in terms of preserving model quality.

A. Performance Impact of Design Optimizations

Following TRiM [8], we demonstrate the impact of each design optimization choice on the speedup performance. Figure 9 displays the performance improvements when design optimizations are gradually incorporated in HEAM system. The baseline is the execution speed of HBM2 in conjunction with bd-PIM, with command address compression technique being applied. The first scenario is *HEAM-BG*, where bg-PIM without LUT is located in each bank group. *Batching* corresponds to when the batching technique is applied to the HEAM system. Finally, *LUT* scheme adds LUT to Batching scenario, reducing direct access to the bank of R table. Applying all the optimization techniques achieves $2.2\times$ higher result than the baseline when the vector size is 512B. HEAM-BG enhances the performance by 34% compared to the baseline. The batching scheme gains 43% of additional speedup by reducing load imbalance issues and satisfying the high demand of pooling size that of the bg-PIM. The root

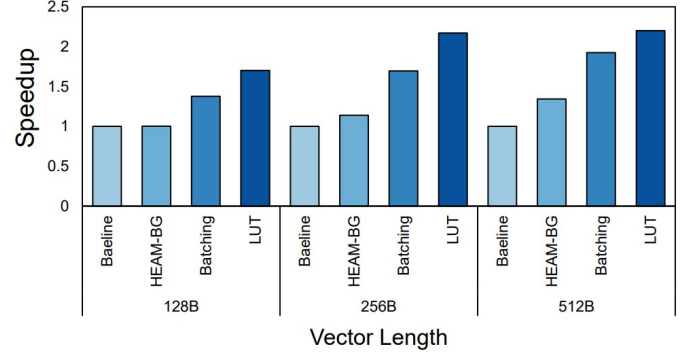


Fig. 9. Performance Impact of Design Optimizations

of the performance benefit of Batching lies in pulling up the underused potential of bank-group-level parallelism. Finally, 14% more speedup is acquired in the LUT scenario, as it reduces the total DRAM access count by effectively utilizing the high temporal locality of the R table. Discussed highlights of each optimization technique increase as the vector length grows, leading to more frequent ACTs within each bank group, creating an environment that fully allows bg-PIM to capitalize its parallelism.

The relatively low speedup with a small vector size primarily results in the underuse of bg-PIM’s parallel processing capabilities, stemming from the low ACT frequency. This impact is further amplified on HEAM-BG’s speedup, as HBM can already conduct parallel embedding lookups effectively for small vector sizes since it possesses abundant channels. However, when batching is applied, total embedding lookups per PIM operation increase, resulting in higher throughput than baseline.

B. Performance Evaluation with Previous NMP Designs

Speedup Comparison. To demonstrate the effectiveness of our proposal, we compare the overall performance of HEAM to the speedup in embedding operation of the previous works [6], [7], [8], [9]. In our experiment, a total of two DIMMs were utilized for previous DIMM-based NMP architectures.

Through the use of a heterogeneous memory system, 2-level PIM structure, and offloading techniques, HEAM achieved the best speedup across all the prior works. Figure 10 shows the relative performance of configurations normalized to Tensor-DIMM, varying vector lengths from 128B to 512B. Compared to the prior works, HEAM achieves $6.2\times$, $4.77\times$, $3.3\times$, $2.13\times$ speedup compared to TensorDIMM, RecNMP, TRiM-G, SPACE when vector length is 512B. Compared to SPACE, which also utilizes a heterogeneous memory system, HEAM’s superior achievement in speedup comes from the utilization of bg-PIM followed by design choices of batching and LUT. However, bank group parallelism’s impact is minimal for short vector lengths due to fewer vector reads per channel, especially when compared to the nearly uniform speedup of the TRiM. This occurs because HBM2 has four times more channels than two DIMMs, leading to underutilized bank group parallelism. With larger vector sizes, HEAM’s performance significantly improves as the internal bandwidth

is better utilized, thanks to more frequent ACT commands. Employing a larger pooling size and larger vector length, a typical trend of recommendation systems in production, would result in full utilization of HEAM's maximal bandwidth.

Relative Energy Consumption. Figure 11 depicts the relative energy consumption of prior works and HEAM, which are normalized to the result of TensorDIMM. As shown in the figure, HEAM saves 58.9%, 45.9%, and 14.1% energy compared to TensorDIMM, RecNMP, and SPACE. HEAM saves 14.2% from SPACE energy consumption, similar to the amount of energy saved compared to TRiM-G.

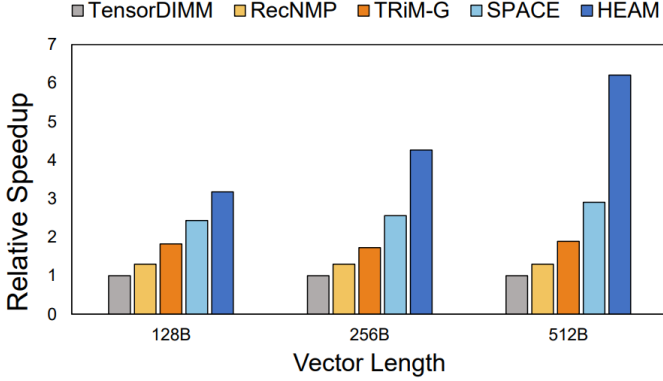


Fig. 10. Performance evaluation on various NMP systems

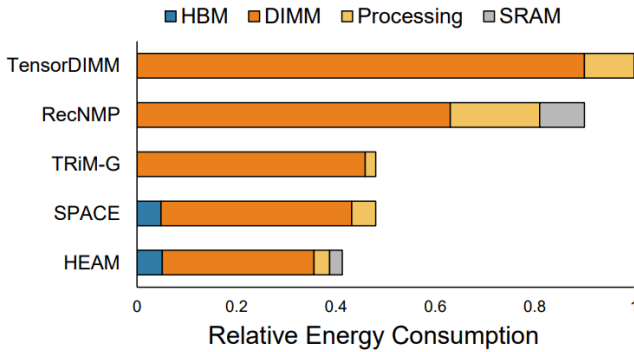


Fig. 11. Relative energy consumption in NMP models

C. Design Overhead

The total area occupied by bg-PIM is $1.66mm^2$ per HBM2 die, which takes a 1.7% portion of each HBM2 die. LUT consists of 20KB SRAM which takes 10% of the total PIM area. Each PIM includes four MAC units, register files for buffer and logic support. The total gate count is 125,740 per each bg-PIM. The energy consumption of LUT accounts for 0.04% of total energy consumed by HEAM, which enables high energy savings from DRAM access. Total area overhead of bd-PIM is $0.37mm^2$ per channel, with gate count of 118,087 each.

D. Assessment of Compositional Embedding Shortcomings

Efficiency of Increasing Hash Collision. To achieve the necessary bandwidth ratio between HBM and DIMM, reducing

the total number of hot vectors should coincide adequately with increased hash collisions. If not sufficiently reduced, the total hot vectors might surpass the capacity of a single HBM stack in production scenarios. For an ideal case, hot vectors would be grouped closely, allowing a quotient hash function to map consecutive hot vectors to the same Q vector. This would reduce the total number of hot vectors inversely proportional to the increase in hash collisions. However, this ideal situation is rare. In the worst-case scenario, the reduction in total hot vectors is minimal, as cold vectors typically outnumber and surround each hot Q vector, leading to only a marginal decrease.

To verify the reduction efficiency, we measured the changes in the number of the hot vectors while modifying hash collision value on public datasets available online [25], [32], [33]. In this experiment, we defined hot vectors as the vectors needed to achieve 80% of the cumulative request. The result is shown in Figure 12 (a). Although the result indicates the hot vectors are not clustered ideally, increasing hash collision still decreases hot vectors to a certain extent, which is enough to meet the bandwidth ratio demand between HBM and DIMM.

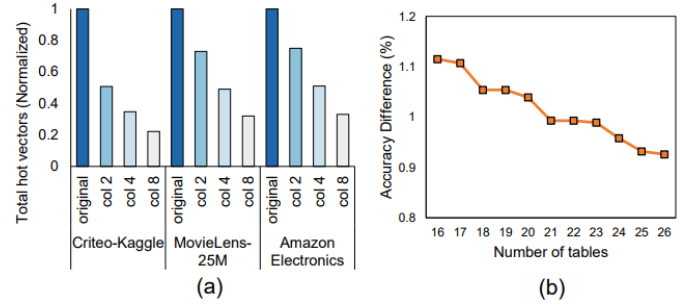


Fig. 12. Compositional embedding shortcoming analysis. (a) Change in the number of hot vectors based on the hash collision value across criteo-kaggle, movielens-25M, amazon electronics. (b) Accuracy difference between the original model and the model trained with compositional embedding by hash collision 4.

Decrease in Model Quality Drop with More Embedding Tables. As more embedding tables are used in the recommendation system, the model quality increases [5]. At the production level, it is known that there are 10s of embedding tables. As the accuracy drop of compositional embedding is due to the mixture of distinctive embeddings [22], applying more embedding tables might resolve the accuracy drop caused when applying the algorithm. To see the effect of embedding tables on the accuracy, we conducted experiments in criteo-kaggle-dataset. Since some tables are used more often than others, we picked randomly the tables to be excluded, averaging the result of 3 experiments. The overall result is shown in Figure 12 (b). By excluding tables from 10 tables to 0 tables, we found that the gap of accuracy drop decreases.

VII. CONCLUSION

We introduce HEAM, a three-tiered memory architecture that comprises DIMM, HBM featuring bd-PIM and bg-PIM and LUT inside bg-PIM. Our system tackles two key challenges in deep learning recommendation system: Model size expansion and Memory-bound operations. We examined the unique

characteristics of compositional embedding and leveraged our findings to boost overall throughput. HEAM effectively resolves the issue of double memory access that arises when applying compositional embedding, resulting in $6.2\times$ performance improvement and 58.9% energy savings compared to the previous NMP architectures tailored for recommendation systems.

REFERENCES

- [1] M. Naumov, D. Mudigere, H.-J. M. Shi, J. Huang, N. Sundaraman, J. Park, X. Wang, U. Gupta, C.-J. Wu, A. G. Azzolini, *et al.*, “Deep learning recommendation model for personalization and recommendation systems,” *arXiv preprint arXiv:1906.00091*, 2019.
- [2] P. Covington, J. Adams, and E. Sargin, “Deep neural networks for youtube recommendations,” in *Proceedings of the 10th ACM conference on recommender systems*, pp. 191–198, 2016.
- [3] H. Steck, L. Baltrunas, E. Elahi, D. Liang, Y. Raimond, and J. Basilico, “Deep learning for recommender systems: A netflix case study,” *AI Magazine*, vol. 42, no. 3, pp. 7–18, 2021.
- [4] U. Gupta, C.-J. Wu, X. Wang, M. Naumov, B. Reagen, D. Brooks, B. Cotel, K. Hazelwood, M. Hempstead, B. Jia, *et al.*, “The architectural implications of facebook’s dnn-based personalized recommendation,” in *2020 IEEE International Symposium on High Performance Computer Architecture (HPCA)*, pp. 488–501, IEEE, 2020.
- [5] M. Zhao, N. Agarwal, A. Basant, B. Gedik, S. Pan, M. Ozdal, R. Komuravelli, J. Pan, T. Bao, H. Lu, *et al.*, “Understanding data storage and ingestion for large-scale deep recommendation model training: Industrial product,” in *Proceedings of the 49th Annual International Symposium on Computer Architecture*, pp. 1042–1057, 2022.
- [6] Y. Kwon, Y. Lee, and M. Rhu, “Tensordimm: A practical near-memory processing architecture for embeddings and tensor operations in deep learning,” in *Proceedings of the 52nd Annual IEEE/ACM International Symposium on Microarchitecture*, pp. 740–753, 2019.
- [7] L. Ke, U. Gupta, B. Y. Cho, D. Brooks, V. Chandra, U. Diril, A. Firoozshahian, K. Hazelwood, B. Jia, H.-H. S. Lee, *et al.*, “Recnmp: Accelerating personalized recommendation with near-memory processing,” in *2020 ACM/IEEE 47th Annual International Symposium on Computer Architecture (ISCA)*, pp. 790–803, IEEE, 2020.
- [8] J. Park, B. Kim, S. Yun, E. Lee, M. Rhu, and J. H. Ahn, “Trim: Enhancing processor-memory interfaces with scalable tensor reduction in memory,” in *MICRO-54: 54th Annual IEEE/ACM International Symposium on Microarchitecture*, pp. 268–281, 2021.
- [9] H. Kal, S. Lee, G. Ko, and W. W. Ro, “Space: locality-aware processing in heterogeneous memory for personalized recommendations,” in *2021 ACM/IEEE 48th Annual International Symposium on Computer Architecture (ISCA)*, pp. 679–691, IEEE, 2021.
- [10] L. Ke, X. Zhang, J. So, J.-G. Lee, S.-H. Kang, S. Lee, S. Han, Y. Cho, J. H. Kim, Y. Kwon, *et al.*, “Near-memory processing in action: Accelerating personalized recommendation with axdim,” *IEEE Micro*, vol. 42, no. 1, pp. 116–127, 2021.
- [11] B. Asgari, R. Hadidi, J. Cao, S.-K. Lim, H. Kim, *et al.*, “Fafnir: Accelerating sparse gathering by using efficient near-memory intelligent reduction,” in *2021 IEEE International Symposium on High-Performance Computer Architecture (HPCA)*, pp. 908–920, IEEE, 2021.
- [12] *High Bandwidth Memory DRAM(HBM1, HBM2)*, JEDEC Standard JESD235D, 2021.
- [13] G. Sethi, B. Acun, N. Agarwal, C. Kozyrakis, C. Trippel, and C.-J. Wu, “Recshard: statistical feature-based memory optimization for industry-scale neural recommendation,” in *Proceedings of the 27th ACM International Conference on Architectural Support for Programming Languages and Operating Systems*, pp. 344–358, 2022.
- [14] D. Mudigere, Y. Hao, J. Huang, Z. Jia, A. Tulloch, S. Sridharan, X. Liu, M. Ozdal, J. Nie, J. Park, *et al.*, “Software-hardware co-design for fast and scalable training of deep learning recommendation models,” in *Proceedings of the 49th Annual International Symposium on Computer Architecture*, pp. 993–1011, 2022.
- [15] E. K. Ardestani, C. Kim, S. J. Lee, L. Pan, J. Axboe, V. Rampersad, B. Agrawal, F. Yu, A. Yu, T. Le, *et al.*, “Supporting massive dlrm inference through software defined memory,” in *2022 IEEE 42nd International Conference on Distributed Computing Systems (ICDCS)*, pp. 302–312, IEEE, 2022.
- [16] L. Ke, U. Gupta, M. Hempstead, C.-J. Wu, H.-H. S. Lee, and X. Zhang, “Hercules: Heterogeneity-aware inference serving for at-scale personalized recommendation,” in *2022 IEEE International Symposium on High-Performance Computer Architecture (HPCA)*, pp. 141–154, IEEE, 2022.
- [17] A. Firoozshahian, J. Coburn, R. Levenstein, R. Nattoji, A. Kamath, O. Wu, G. Grewal, H. Aepala, B. Jakka, B. Dreyer, *et al.*, “Mtia: First generation silicon targeting meta’s recommendation systems,” in *Proceedings of the 50th Annual International Symposium on Computer Architecture*, pp. 1–13, 2023.
- [18] W. Zhao, J. Zhang, D. Xie, Y. Qian, R. Jia, and P. Li, “Aibox: Ctr prediction model training on a single node,” in *Proceedings of the 28th ACM International Conference on Information and Knowledge Management*, pp. 319–328, 2019.
- [19] H.-J. M. Shi, D. Mudigere, M. Naumov, and J. Yang, “Compositional embeddings using complementary partitions for memory-efficient recommendation systems,” in *Proceedings of the 26th ACM SIGKDD International Conference on Knowledge Discovery & Data Mining*, pp. 165–175, 2020.
- [20] A. A. Ginart, M. Naumov, D. Mudigere, J. Yang, and J. Zou, “Mixed dimension embeddings with application to memory-efficient recommendation systems,” in *2021 IEEE International Symposium on Information Theory (ISIT)*, pp. 2786–2791, IEEE, 2021.
- [21] C. Yin, B. Acun, C.-J. Wu, and X. Liu, “Tt-rec: Tensor train compression for deep learning recommendation models,” *Proceedings of Machine Learning and Systems*, vol. 3, pp. 448–462, 2021.
- [22] F. Lyu, X. Tang, H. Zhu, H. Guo, Y. Zhang, R. Tang, and X. Liu, “Optembed: Learning optimal embedding table for click-through rate prediction,” in *Proceedings of the 31st ACM International Conference on Information & Knowledge Management*, pp. 1399–1409, 2022.
- [23] K. Weinberger, A. Dasgupta, J. Langford, A. Smola, and J. Attenberg, “Feature hashing for large scale multitask learning,” in *Proceedings of the 26th annual international conference on machine learning*, pp. 1113–1120, 2009.
- [24] W.-C. Kang, D. Z. Cheng, T. Yao, X. Yi, T. Chen, L. Hong, and E. H. Chi, “Learning to embed categorical features without embedding tables for recommendation,” in *Proceedings of the 27th ACM SIGKDD Conference on Knowledge Discovery & Data Mining*, pp. 840–850, 2021.
- [25] CriteoLabs. 2014, “Kaggle display advertising challenge dataset.” [Online]. Available : <https://jmcauley.ucsd.edu/data/amazon/>.
- [26] V. J. Reddi, C. Cheng, D. Kanter, P. Mattson, G. Schmuelling, C.-J. Wu, B. Anderson, M. Breughe, M. Charlebois, W. Chou, *et al.*, “Mlperf inference benchmark,” in *2020 ACM/IEEE 47th Annual International Symposium on Computer Architecture (ISCA)*, pp. 446–459, IEEE, 2020.
- [27] S. Li, Z. Yang, D. Reddy, A. Srivastava, and B. Jacob, “Dramsim3: A cycle-accurate, thermal-capable dram simulator,” *IEEE Computer Architecture Letters*, vol. 19, no. 2, pp. 106–109, 2020.
- [28] J. Sim, A. R. Alameldeen, Z. Chishti, C. Wilkerson, and H. Kim, “Transparent hardware management of stacked dram as part of memory,” in *2014 47th Annual IEEE/ACM International Symposium on Microarchitecture*, pp. 13–24, IEEE, 2014.
- [29] C. C. Chou, A. Jaleel, and M. K. Qureshi, “Cameo: A two-level memory organization with capacity of main memory and flexibility of hardware-managed cache,” in *2014 47th Annual IEEE/ACM International Symposium on Microarchitecture*, pp. 1–12, IEEE, 2014.
- [30] C. Chou, A. Jaleel, and M. K. Qureshi, “Bear: Techniques for mitigating bandwidth bloat in gigascale dram caches,” *ACM SIGARCH Computer Architecture News*, vol. 43, no. 3S, pp. 198–210, 2015.
- [31] N. Muralimanohar, R. Balasubramonian, and N. P. Jouppi, “Cacti 6.0: A tool to model large caches,” *HP laboratories*, vol. 27, p. 28, 2009.
- [32] F. M. Harper and J. A. Konstan, “The movielens datasets: History and context,” *Acmm transactions on interactive intelligent systems (tiis)*, vol. 5, no. 4, pp. 1–19, 2015.
- [33] M. Wan, J. Ni, R. Misra, and J. McAuley, “Addressing marketing bias in product recommendations,” in *Proceedings of the 13th international conference on web search and data mining*, pp. 618–626, 2020.